AMERICAN SOCIETY FOR MICROBIOLOGY | Journal of Virology®

VACCINES AND ANTIVIRAL AGENTS

Novel Modified Vaccinia Virus Ankara Vector Expressing Anti-apoptotic Gene *B13R* Delays Apoptosis and Enhances Humoral Responses

Lynette S. Chea,[a,b] Linda S. Wyatt,[c] Sailaja Gangadhara,[a,b] Bernard Moss,[c] Rama R. Amara[a,b]

[a]Department of Microbiology and Immunology, Emory University School of Medicine, Atlanta, Georgia, USA
[b]Division of Microbiology and Immunology, Emory Vaccine Center, Yerkes National Primate Research Center, Emory University, Atlanta, Georgia, USA
[c]Laboratory of Viral Diseases, National Institute of Allergy and Infectious Diseases, National Institutes of Health, Bethesda, Maryland, USA

ABSTRACT Modified vaccinia virus Ankara (MVA), an attenuated poxvirus, has been developed as a potential vaccine vector for use against cancer and multiple infectious diseases, including human immunodeficiency virus (HIV). MVA is highly immunogenic and elicits strong cellular and humoral responses in preclinical models and humans. However, there is potential to further enhance the immunogenicity of MVA, as MVA-infected cells undergo rapid apoptosis, leading to faster clearance of recombinant antigens and potentially blunting a greater response. Here, we generated MVA-*B13R* by replacing the fragmented *181R*/*182R* genes of MVA with a functional anti-apoptotic gene, *B13R*, and confirmed its anti-apoptotic function against chemically induced apoptosis *in vitro*. In addition, MVA-*B13R* showed a significant delay in induction of apoptosis in muscle cells derived from mice and humans, as well as in plasmacytoid dendritic cells (pDCs) and CD141$^+$ DCs from rhesus macaques, compared to the induction of apoptosis in MVA-infected cells. MVA-*B13R* expressing simian immunodeficiency virus (SIV) Gag and Pol and HIV envelope (SHIV) (MVA-*B13R*/SHIV) produced higher levels of envelope in the supernatants than MVA/SHIV-infected DF-1 cells *in vitro*. Immunization of BALB/c mice showed induction of higher levels of envelope-specific antibody-secreting cells and memory B cells, higher IgG antibody titers, and better persistence of antibody titers with MVA-*B13R*/SHIV than with MVA/SHIV. Gene set enrichment analysis of draining lymph node cells from day 1 after immunization showed negative enrichment for interferon responses in MVA-*B13R*/SHIV-immunized mice compared to the responses in MVA/SHIV-immunized mice. Taken together, these results demonstrate that restoring *B13R* functionality in MVA significantly delays MVA-induced apoptosis in muscle and antigen-presenting cells *in vitro* and augments vaccine-induced humoral immunity in mice.

IMPORTANCE MVA is an attractive viral vector for vaccine development due to its safety and immunogenicity in multiple species and humans even under conditions of immunodeficiency. Here, to further improve the immunogenicity of MVA, we developed a novel vector, MVA-*B13R*, by replacing the fragmented anti-apoptotic genes *181R*/*182R* with a functional version derived from vaccinia virus, *B13R*. Our results show that MVA-*B13R* significantly delays apoptosis in antigen-presenting cells and muscle cells *in vitro* and augments vaccine-induced humoral immunity in mice, leading to the development of a novel vector for vaccine development against infectious diseases and cancer.

KEYWORDS MVA, antibody responses, modified vaccinia virus Ankara, poxvirus, vaccine, viral vector

Citation Chea LS, Wyatt LS, Gangadhara S, Moss B, Amara RR. 2019. Novel modified vaccinia virus Ankara vector expressing anti-apoptotic gene *B13R* delays apoptosis and enhances humoral responses. J Virol 93:e01648-18. https://doi.org/10.1128/JVI.01648-18.

Editor Frank Kirchhoff, Ulm University Medical Center

Address correspondence to Rama R. Amara, ramara@emory.edu.

Received 18 September 2018
Accepted 17 November 2018
Accepted manuscript posted online 12 December 2018
Published 19 February 2019

The goals of an effective vaccine are to induce robust and durable humoral and cellular immunity to prevent and control pathogenic infection. To date, attenuated poxviruses, such as ALVAC, NYVAC, and modified vaccinia virus Ankara (MVA), have been explored as vaccine vectors for use against multiple infectious diseases and even cancers. MVA is a highly attenuated derivative of vaccinia virus, with an excellent safety record as well as proven sustained immunogenicity in humans and most mammals despite being replication incompetent (1). The genetic attenuation achieved by MVA was due to over 570 passages of vaccinia virus in chicken embryo fibroblast cells, which led to approximately 12% of its genome being deleted or fragmented, with many of the lost genes being host range and host immune-modulatory genes. For use as a vector, the MVA genome can stably accommodate recombinant genes as large as 25 kb, and due to the defect at the late stage of virion assembly, late gene and recombinant gene expression can occur undeterred (2, 3).

These characteristics make MVA a promising vector for use in vaccinations. Vaccine regimens utilizing MVA have undergone numerous preclinical and phase I/II clinical trials for infectious diseases, including human immunodeficiency virus (HIV), Ebola, and tuberculosis, as well as for a variety of cancers (4–17). These studies have demonstrated that MVA is capable of inducing antigen-specific cellular and humoral responses in participants. However, there still remains the need to induce better responses from MVA immunizations, as not all participants induced antigen-specific immune responses even after multiple immunizations (7, 13, 15). A vaccine capable of eliciting a more robust response has the potential to be used as a prophylactic vaccine for preventing infections or as a therapeutic one to help against disease progression.

Improving the immunogenicity of MVA by modulating the viral genome has been pursued by many groups, namely through the deletion of immunomodulatory genes (18–24). This strategy includes deletion of the anti-apoptotic *F1L* gene in MVA in order to increase the rate of apoptosis induction via the intrinsic pathway (22). Apoptosis is a form of programmed cell death mediated by host caspase enzymes, with characteristic physiological features like cell shrinking, nuclear condensation and fragmentation, membrane blebbing, and budding of apoptotic bodies (25, 26). The immunogenicity of apoptotic cells may stem from prolonged storage of the cell-associated antigens within dendritic cells (DCs) that capture and present the antigens (27). The persistence of antigen by apoptotic cells and, thus, its immunogenicity could in part be attributed to its targeted delivery to recycling endosomes and ability to recruit and stimulate immune cells.

While it is clear that apoptotic cells are immunogenic, the kinetics of their generation may play an important role in improving antigen-specific responses. Using a canarypox vector for HIV vaccination, Fang et al. expressed two vaccinia virus genes that reduced the level of apoptosis, leading to enhanced HIV-1 pseudovirion production *in vitro* (28). Additionally, an *in vivo* study using DNA-delivered mutated caspase 2 or 3 showed delayed apoptosis induction and increased immunogen expression before the generation of apoptotic bodies (29). The mutated caspases performed similarly to an adjuvant, as the authors observed enhanced $CD4^+$ and $CD8^+$ T cell responses compared to the response to delivery of wild-type caspases. Modifying the MVA vector to delay the induction of apoptosis during vaccination has the potential to improve antigen-specific immune responses by allowing for more immunogen production before apoptosis and enhancing the ability of DCs to generate memory B and T cells.

Here, we aimed to enhance the immunogenicity of the MVA vector by delaying apoptosis induction through the expression of a vaccinia virus-derived anti-apoptotic gene. *B13R* is a gene in the Western Reserve (WR) strain of vaccinia virus that has been shown to protect against apoptosis via the extrinsic pathway in cells infected with vaccinia virus (30). The gene product, serpin-2 (SPI-2), is expressed early during infection and is related to the serine protease inhibitor family of proteins (31, 32). SPI-2 and its ortholog in cowpox, cytokine response modifier A (CrmA), are the best studied of the poxvirus serpins. CrmA inhibits interleukin-1β (IL-1β)-converting enzyme (caspase 1) and prevents apoptosis (32). It has also been shown to block apoptosis initiated by

the Fas and tumor necrosis factor (TNF) receptors by potently inhibiting caspase 8-mediated apoptosis (33). Additionally, CrmA has the ability to abrogate the effects of granzyme B released from cytotoxic T lymphocytes (CTLs) *in vitro* (34). CrmA thus has the ability to prevent apoptosis initiated by the extrinsic and CTL-mediated pathways. However, the ortholog of WR *B13R* in MVA is fragmented (*181R*/*182R*) and rendered nonfunctional (35). In this study, we have replaced the fragmented genes in MVA with a functional copy of *B13R* from the WR strain to delay the onset of apoptosis, increase antigen load and persistence, and improve the adaptive immune response. Our data show that MVA expressing the full-length *B13R*, MVA-*B13R*, is capable of delaying apoptosis of infected cells compared to the induction of apoptosis by MVA and that this leads to enhanced humoral responses in mice following vaccination.

RESULTS

MVA-induced cell death is mediated by caspases. To determine the degree of apoptosis induced by MVA, we infected HeLa cells at a multiplicity of infection (MOI) of 3 and measured caspase 3 activation in MVA-infected cells by staining for the early vaccinia virus E3 protein, to assess MVA infection (MVA-positive [MVA^+] cells), and for active caspase 3 (Fig. 1A). We used active caspase 3 to detect cells undergoing apoptosis as it is a main downstream effector caspase in the apoptosis cascade that is activated upon cleavage from its inactive pro-caspase 3 form by initiator caspase 8 or 9. In addition, we stained cells with an amine-reactive dye, LIVE/DEAD near-IR dead cell stain, to detect membrane permeability, which denotes cells undergoing later stages of apoptosis (also active caspase 3 positive [active caspase 3^+]) or necrosis (active caspase 3 negative [active caspase 3^-]). Through 88 h after infection, MVA infection significantly increased caspase 3 activation, indicating caspase-dependent cell death induced by MVA (Fig. 1B). To further confirm the role of cellular caspases during MVA-induced cell death, we added inhibitors specific for individual caspases or for all caspases during MVA infection and determined caspase 3 activation levels at 50 h postinfection. Inhibition by a pan-caspase inhibitor, as well as individual caspases like caspases 3, 4, 6, and 8, led to reduced activation of caspase 3 during MVA infection compared to its activation in the vehicle-treated MVA-infected cells, indicating a role for multiple caspases in MVA-induced cell death (Fig. 1C).

MVA-induced apoptosis is delayed by *B13R* expression. After confirming the role of caspases in MVA-mediated cell death, we expressed the *B13R* gene derived from WR vaccinia virus to determine whether *B13R* expression during MVA infection would lead to a delay in cell death (Fig. 1D). The MVA genes *181R*/*182R* in MVA comprise the nonfunctional disrupted orthologs of the WR *B13R* gene, and we initially removed them via homologous recombination with a green fluorescent protein (GFP)-encoding PCR product to generate MVA-GFPΔ*181R*/*182R*. The GFP gene was then replaced with the full-length WR *B13R* gene, generating MVA-*B13R*. A Western blot analysis of MVA-*B13R*-infected cell lysates showed a band of the expected size of 38.5 kDa for MVA-*B13R*, confirming its expression (Fig. 1E). WR vaccinia virus-infected cells served as the positive control, and the absence of a band in MVA- and mock-infected DF-1 cells (cell line permissive to MVA replication) confirmed *B13R* expression by our novel construct, MVA-*B13R*.

To confirm functionality of the *B13R* gene, we infected HeLa cells with MVA-*B13R* and subsequently treated the infected cells with TNF-α and cycloheximide to chemically induce apoptosis. As expected, TNF-α and cycloheximide treatment induced strong caspase 3 activation in cells as early as 24 h. However, infection with MVA-*B13R* significantly reduced caspase 3 activation, by as much as 30%, at 24 h posttreatment (Fig. 1F). These data indicate that *B13R* expression is capable of delaying the activation of the apoptotic process. To address whether the expression of *B13R* would lead to enhanced replication of the virus, we determined the growth curves of MVA or MVA-*B13R* by infecting DF-1 cells at an MOI of 0.05 and measuring viral titers from cell lysates. The growth curves for the viruses did not differ over time, indicating that *B13R* expression did not affect the replication and spread of MVA in DF-1 cells (Fig. 1G).

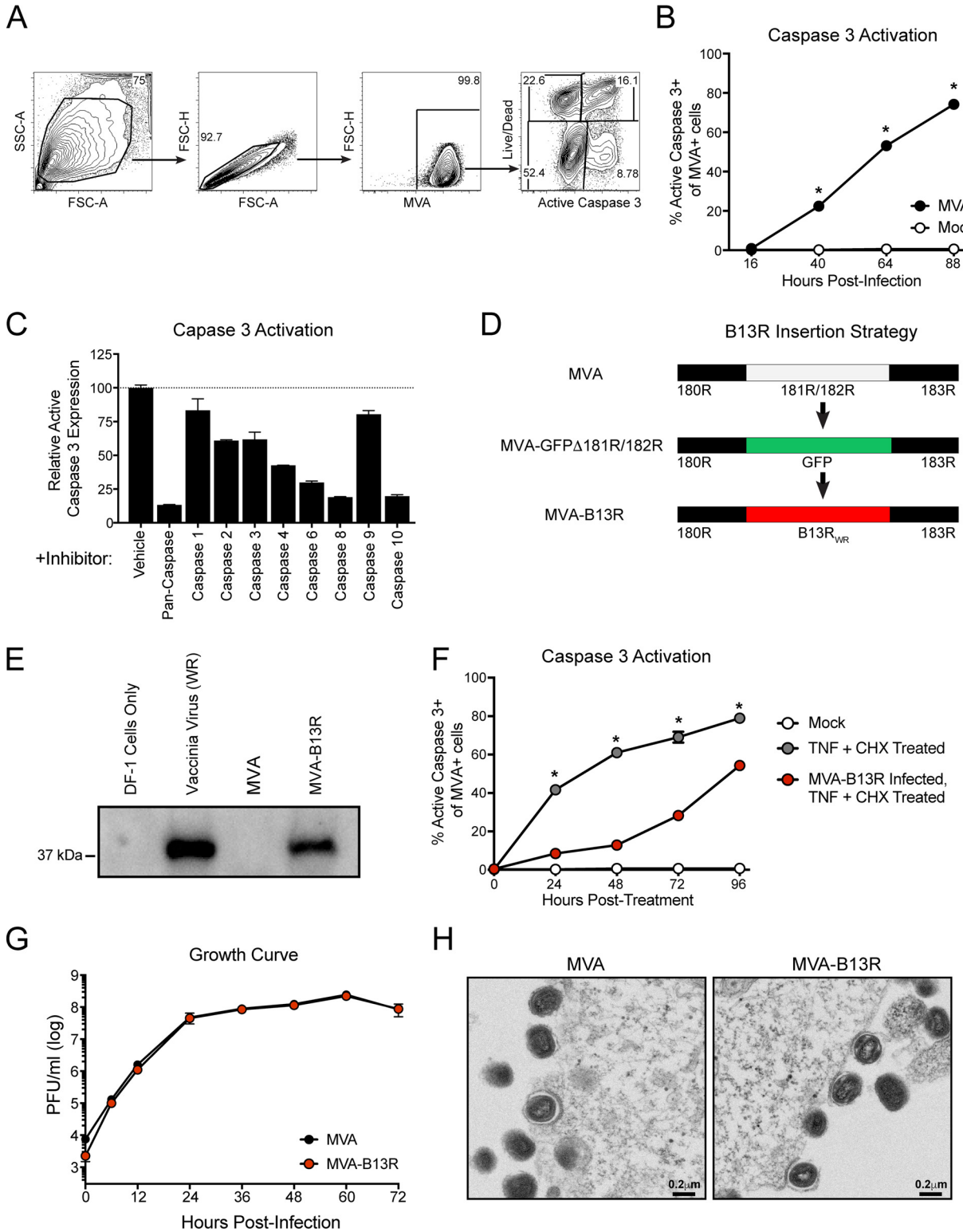

FIG 1 *B13R* expression by MVA during infection delays apoptosis of infected cells. HeLa cells were infected with MVA at an MOI of 3, and active caspase 3 expression of MVA-infected cells was detected by flow cytometry. (A) Representative flow gating to determine the viability of MVA-infected cells: doublet exclusion followed by vaccinia virus E3 protein expression for MVA^+ cells and LIVE/DEAD and active caspase 3 staining for viability. SSC, side scatter; FSC, forward scatter. (B) Percentages of active caspase 3^+ cells among MVA^+ cells. (C) HeLa cells were infected with MVA at an MOI of 2 for 2 h, and then inoculum was replaced with fresh medium containing indicated caspase inhibitors or DMSO (vehicle control) at 100 μM. Active caspase 3 expression was detected among MVA^+ cells at 48 h postinfection and normalized to the results for vehicle control. (D) Schematic of *B13R* insertion strategy: *181R/182R* gene from the MVA genome was replaced via homologous recombination with GFP. GFP was then replaced with *B13R* derived from Western Reserve (WR) strain of vaccinia virus to generate MVA-*B13R*. (E) Western blot analysis of DF-1 cell

(Continued on next page)

Additionally, electron microscopy (EM) imaging of infected cells showed no structural differences in budding, mature virions produced by the two viruses at 24 h after infection (Fig. 1H). Thus, *B13R* expression during the course of MVA infection is able to delay cell death induction without interfering with the growth rate or structure of the virus.

MVA-*B13R* delays death of infected cells compared to MVA. After confirming that *B13R* expression is capable of delaying chemically induced cell death, we compared the kinetics of cell death between MVA-*B13R* and MVA. MVA infection resulted in strong activation of caspase 3 in HeLa, RD, and C2C12 cell lines. Kinetic analysis of HeLa cells infected at an MOI of 2 demonstrated significant delay of caspase 3 activation by MVA-*B13R* compared to the results for MVA, beginning at 36 h after infection (Fig. 2A). Interestingly, MVA-*B13R* infection significantly increased the frequency of necrotic cells, e.g., cells undergoing nonapoptotic cell death (Fig. 2A). We performed the same analysis in RD cells, a human muscle cell line derived from a patient's rhabdomyosarcoma, as immunizations are typically administered through the intramuscular route. At an MOI of 3 for infections, we again saw a delay in caspase 3 activation by MVA-*B13R* in the RD cells (Fig. 2B). Additionally, as we aimed to perform immunogenicity studies in a mouse model, we used a mouse myoblast cell line, C2C12, to test the effect of *B13R* expression during MVA infection. The MOI used for the C2C12 cell line was lowered to 0.3 to achieve approximately 50% infection, as greater amounts of virus caused rapid cell death with both virus strains. The reduced level of infectivity allowed us to detect lowered caspase 3 activation, as well as increased cell necrosis, over time for MVA-*B13R* compared to the results for MVA, similar to what was observed during infection in HeLa cells (Fig. 2C).

As the next ideal preclinical model that we hope to test the immunogenicity of MVA-*B13R* in is rhesus macaques, we assessed how MVA-*B13R* would influence the viability of immune cells from rhesus macaques. Peripheral blood mononuclear cells (PBMCs) from naive rhesus macaques were infected *ex vivo* with MVA or MVA-*B13R* at an MOI of 3 and stained to assess MVA infection and viability among various cell subsets by flow cytometry (Fig. 2D to G). We first determined the levels of MVA infectivity in different immune cell subsets (Fig. 2F). Plasmacytoid DCs (pDCs) (Lin^- $HLA\text{-}DR^+$ $CD11c^-$ $CD123^+$), followed by CD141 (BDCA-3)$^+$ DCs (Lin^- $HLA\text{-}DR^+$ $CD11c^+$ $CD141^+$ $CD1c^-$) and CD1c (BDCA-1)$^+$ DCs (Lin^- $HLA\text{-}DR^+$ $CD11c^+$ $CD1c^+$ $CD141^-$) were among the more highly infected subsets, with 50 to 95% infectivity. B cells ($HLA\text{-}DR^+$ $CD20^+$) and $CD16^+$ $CD14^-$ (Lin^- $HLA\text{-}DR^+$) cells were moderately infected, with infectivity ranging from about 15% to 35%. Both $CD8^+$ and $CD4^+$ T cells showed low levels of infection, with a range of 0.5 to 10% infection.

Given the important role antigen-presenting cells (APCs) play in instigating immune responses and the higher levels of infectivity observed in these subsets, we focused on the effect of MVA infection on DCs. pDCs play an important role for antiviral responses through rapid release of type I interferons (IFNs) upon activation and antigen presentation capabilities through major histocompatibility complex (MHC) classes I and II (36, 37). Here, we observed a decrease in caspase 3 activation for MVA-*B13R*-infected pDCs compared to its activation in MVA-infected cells (Fig. 2G). $CD141^+$ DCs have high expression levels of type I IFNs, IL-12p70, and Toll-like receptor 3 (TLR3), have the capacity to induce T helper 1 cell responses, and can cross-present efficiently to cytotoxic T cells (38–41). Here, $CD141^+$ DCs that were infected with MVA exhibited a higher frequency of caspase 3 activation than did MVA-*B13R*-infected cells from the

FIG 1 Legend (Continued)
lysates infected with WR strain, MVA, or MVA-*B13R* at an MOI of 0.5 at 24 h after infection to detect *B13R* expression. (F) HeLa cells were mock infected or infected with MVA-*B13R* for 16 h at an MOI of 3. Cells were then treated with 25 ng/ml TNF-α and 5 μg/ml cycloheximide (CHX), and caspase 3 activation among MVA^+ cells was determined. (G) DF-1 cells were infected at an MOI of 0.05 with MVA or MVA-*B13R*. At indicated times after infection, cell lysates were harvested to determine viral titers by plaque assay. (H) DF-1 cells were infected at an MOI of 0.25 with MVA or MVA-*B13R* and imaged by electron microscopy at 24 h postinfection. For panels B, C, F, and G, data are mean values $\pm$ standard errors of the means (SEM) from duplicate samples. Data are representative of two or more independent experiments. *, $P < 0.05$.

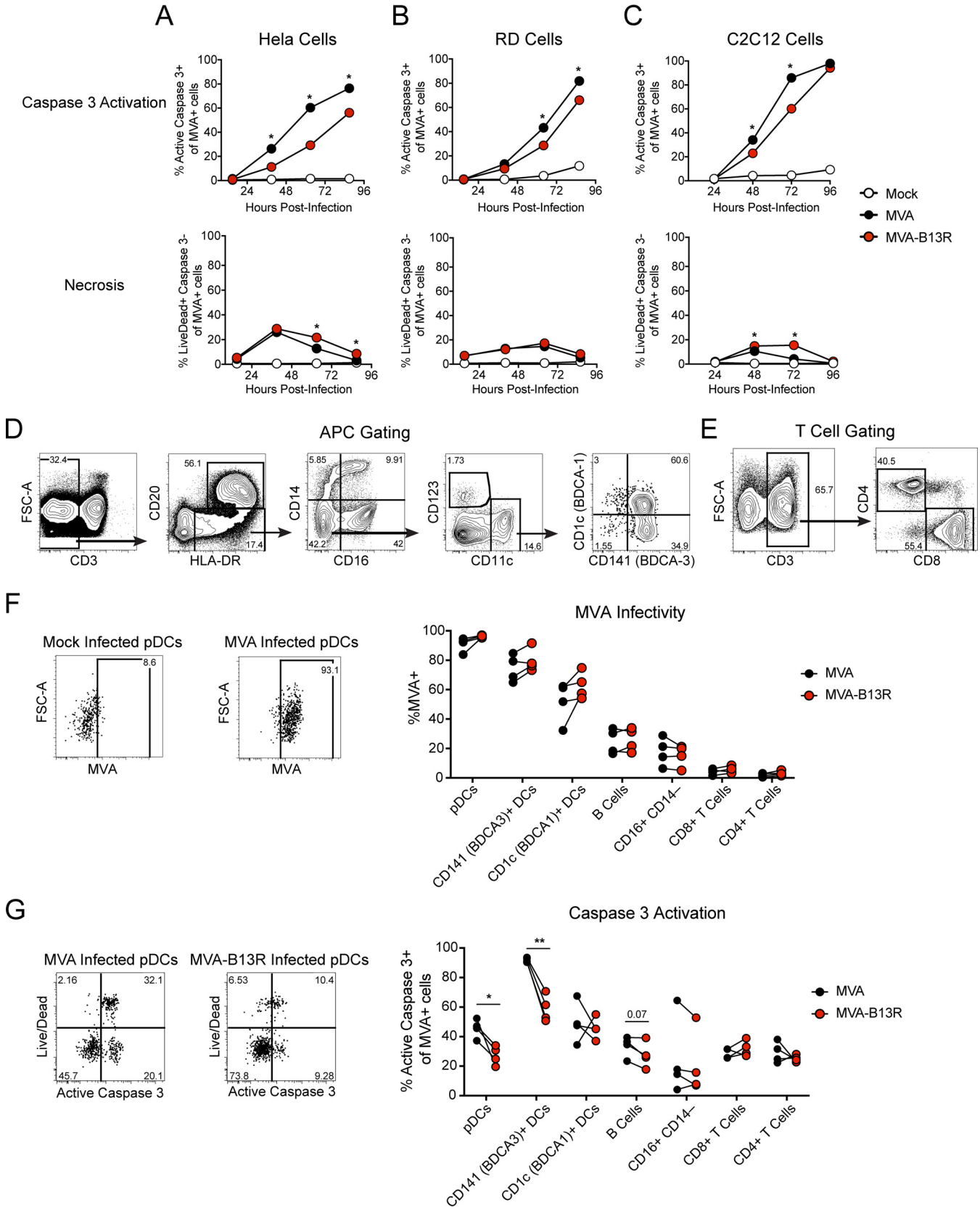

FIG 2 MVA-*B13R* delays cell death of infected cells compared to MVA. (A to C) Kinetics of caspase 3 activation and rates of necrosis of mock-, MVA-, or MVA-*B13R*-infected HeLa cells (MOI of 2) (A), RD cells (a human muscle cell line; MOI of 3) (B), and C2C12 cells (a mouse myoblast cell line; MOI of 0.3) (C). (D to G) PBMCs from rhesus macaques were coincubated with MVA or MVA-*B13R* (MOI of 3) and analyzed by flow cytometry to detect MVA$^+$ cell subsets and

(Continued on next page)

same animal, indicating better viability of these cells after MVA-*B13R* infection, similar to that observed in pDCs (Fig. 2G). As B cells are APCs, as well as the source of antigen-specific antibodies, we assessed B cell viability after MVA infection and saw a trend for improved viability after infection with MVA-*B13R* (Fig. 2G). The remaining APC and T cell subsets did not demonstrate differences in viability after MVA-*B13R* infection relative to the results with MVA (Fig. 2G). Together, these data indicate the possibility that MVA-*B13R*-based vaccinations *in vivo* can significantly influence the viability of APCs, which would substantially shape the adaptive immune response.

Generation of MVA/SHIV and MVA-*B13R*/SHIV. In pursuing our goal to generate a viral vector for immunogenicity studies, we generated recombinant MVA and MVA-*B13R* viruses that express simian immunodeficiency virus (SIV) Gag and Pol and HIV envelope (Env) (SHIV) antigens (Fig. 3A). For both viral strains, we inserted the SIVmac239-derived Gag and Pol genes into the deletion III site and the clade C HIV Env 1086C gene between essential genes of the viral genomes, resulting in viruses expressing SHIV antigens. We confirmed dual expression of SIV Gag and HIV Env by infecting DF-1 cells and staining with antibodies specific to these proteins for flow cytometry (Fig. 3B). More than 85% of the infected cells expressed Gag (Gag^+) and Env, and about 90% of the Gag^+ cells coexpressed Env (Fig. 3B). In addition, we performed Western blot analysis of infected cell lysates to confirm the sizes of the expressed proteins, which revealed the presence of Gag and Env proteins at the expected sizes in cell lysates (Fig. 3C). To test whether there was a difference in the levels of protein expression between the two recombinant vectors over time, we performed a kinetic analysis over 96 h after infection for Env expression in cell lysates, as well as in the supernatants, as these constructs are designed to make SHIV virus-like particles (VLPs). Interestingly, Env production through the course of infection appeared to be higher in the MVA-*B13R*/SHIV-infected-cell lysates than in MVA/SHIV-infected-cell lysates, particularly in the supernatant (Fig. 3D). Using infected DF-1 cells from the same time points, we determined that the level of caspase 3 activation was significantly lower in the MVA-*B13R*/SHIV-infected cells than in MVA/SHIV-infected cells, with a concomitant increase in necrosis (Fig. 3E). This may indicate the ability of MVA-*B13R* to produce more antigen through its prolonging of the viability of infected cells.

MVA-*B13R*/SHIV induces higher and more durable Env-specific humoral responses than MVA/SHIV. To determine the immunogenicity of MVA-*B13R*/SHIV *in vivo*, we immunized BALB/c mice intramuscularly with either MVA/SHIV or MVA-*B13R*/SHIV at a dose of 10^7 PFU at weeks 0 and 4 (Fig. 4A). To determine antigen-specific humoral immunity, we focused our analyses on the period after the booster immunization and measured the Env-specific antibody-secreting cells (ASCs) in the spleen at week 5, Env-specific IgG titers in serum at weeks 5 to 8, and memory B cells (MBCs) in the spleen at week 8. Impressively, the MVA-*B13R*/SHIV-immunized mice induced approximately 3-fold-higher numbers of Env-specific ASCs than the MVA/SHIV-immunized mice (Fig. 4B). This was associated with significantly higher levels of Env-specific IgG titers detected in the serum of MVA-*B13R*/SHIV-immunized mice at weeks 5 and 6 (Fig. 4C). Serum titers continued to be higher for MVA-*B13R*/SHIV-immunized mice at week 8. Additionally, we saw less contraction of serum titers from week 5 to week 8 for MVA-*B13R*/SHIV-immunized mice (Fig. 4D). Impressively, at week 8, we also saw an increased frequency of Env-specific MBCs detected in the spleens of MVA-*B13R*/SHIV-immunized mice compared to the results for MVA/SHIV-immunized mice (Fig. 4E). Taken together, our data demonstrate the ability of MVA-*B13R*/SHIV to induce greater

FIG 2 Legend (Continued)
viability. (D) Representative gating strategy of APC subsets: B cells ($CD3^-$ $CD20^+$ $HLA\text{-}DR^+$), $CD16^+$ $CD14^-$ cells, pDCs (Lin^- $HLA\text{-}DR^+$ $CD11c^-$ $CD123^+$), $CD141^+$ DCs (Lin^- $HLA\text{-}DR^+$ $CD11c^+$ $CD141^+$ $CD1c^-$), and $CD1c^+$ DCs (Lin^- $HLA\text{-}DR^+$ $CD11c^+$ $CD1c^+$ $CD141^-$). (E) Representative gating strategy of $CD4^+$ and $CD8^+$ T cells. (F) Representative MVA staining of mock- or MVA-infected pDCs and percentages of MVA and MVA-*B13R* infection for various cell subsets. Lines indicate matched samples. (G) Left, representative viability staining of MVA- or MVA-*B13R*-infected pDCs with active caspase 3 and LIVE/DEAD; right, percentages of active caspase 3^+ cells among MVA^+ cell subsets (lines indicate matched samples). For panels A to C, data are mean values ± SEM from duplicate samples and are representative of two or more independent experiments. Exact *P* values are reported for some data; *, $P < 0.05$; **, $P < 0.01$.

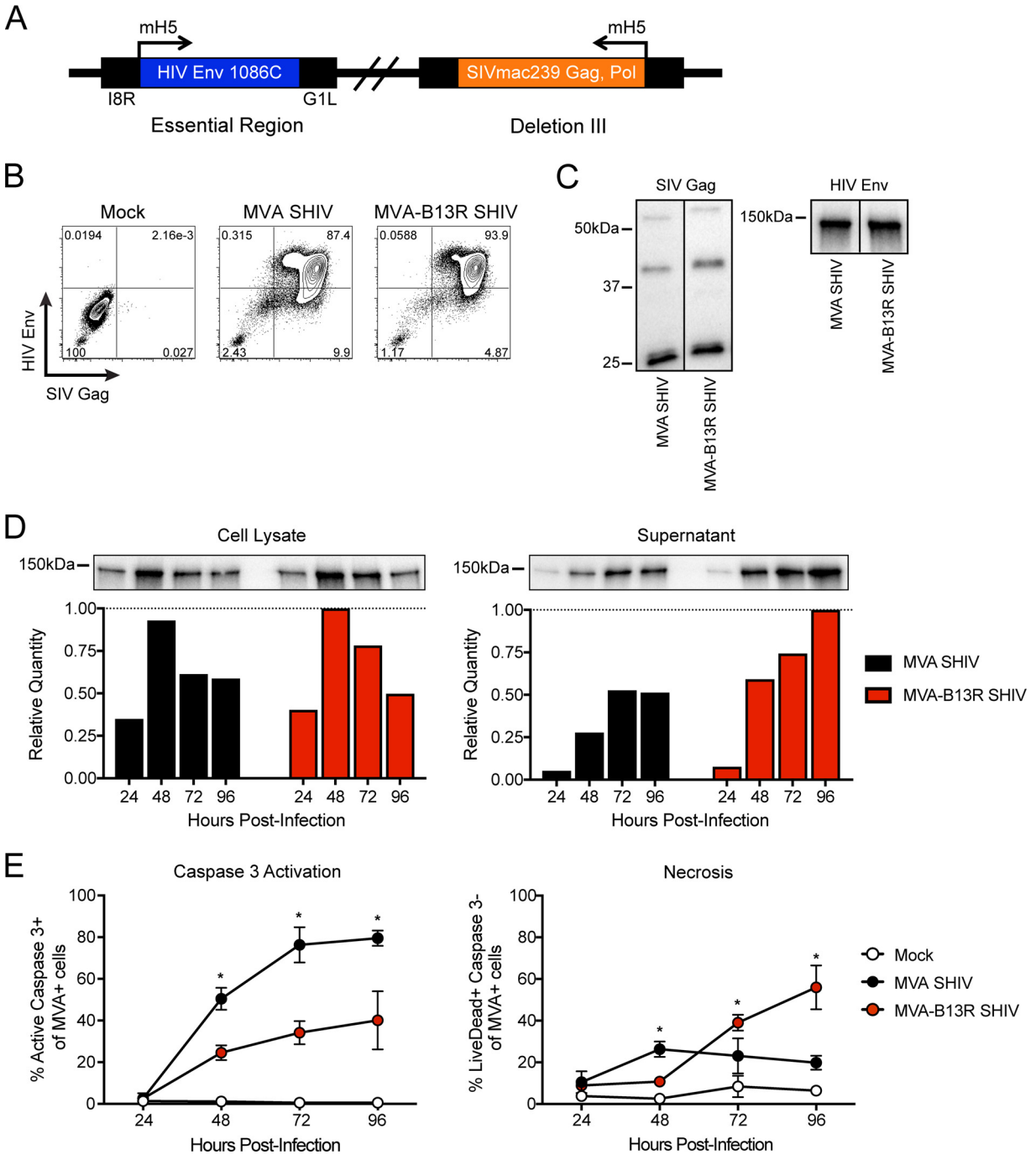

FIG 3 Generation of recombinant MVAs expressing HIV Env 1086C and SIV Gag. (A) Schematic showing insertion sites for HIV Env and SIVmac239 Gag and Pol genes in MVA genomes to generate SHIV constructs. Both gene cassettes are under the control of an independent early/late vaccinia virus promoter, modified H5 (mH5). (B) Flow cytometry confirmed dual expression of SIV Gag and HIV Env from MVA/SHIV and MVA-*B13R*/SHIV constructs at 36 h after infection of DF-1 cells. (C) Western blotting confirmed expression of SIV Gag and HIV Env from MVA/SHIV- and MVA-*B13R*/SHIV-infected DF-1 cell lysates at 48 h after infection at an MOI of 0.05. (D, E) DF-1 cells were infected with MVA/SHIV or MVA-*B13R*/SHIV at an MOI of 0.05. (D) Cell lysates and supernatant were harvested at indicated time points for detection of HIV Env by Western blotting. Relative quantities of each band as determined by densitometry are presented below Western blot images. Representative images from two independent experiments are shown. (E) Cells were harvested at indicated time points and percentages of caspase 3 activation and necrosis were detected for MVA^+ cells. For panel E, data are mean values ± SEM from two independent experiments. *, $P < 0.05$.

and more durable Env-specific humoral responses than MVA/SHIV in our prime/boost vaccination regimen.

We additionally measured the MVA-specific IgG serum titers and observed no difference between the groups at week 5 or 6 (Fig. 4F). When we compared the ratio

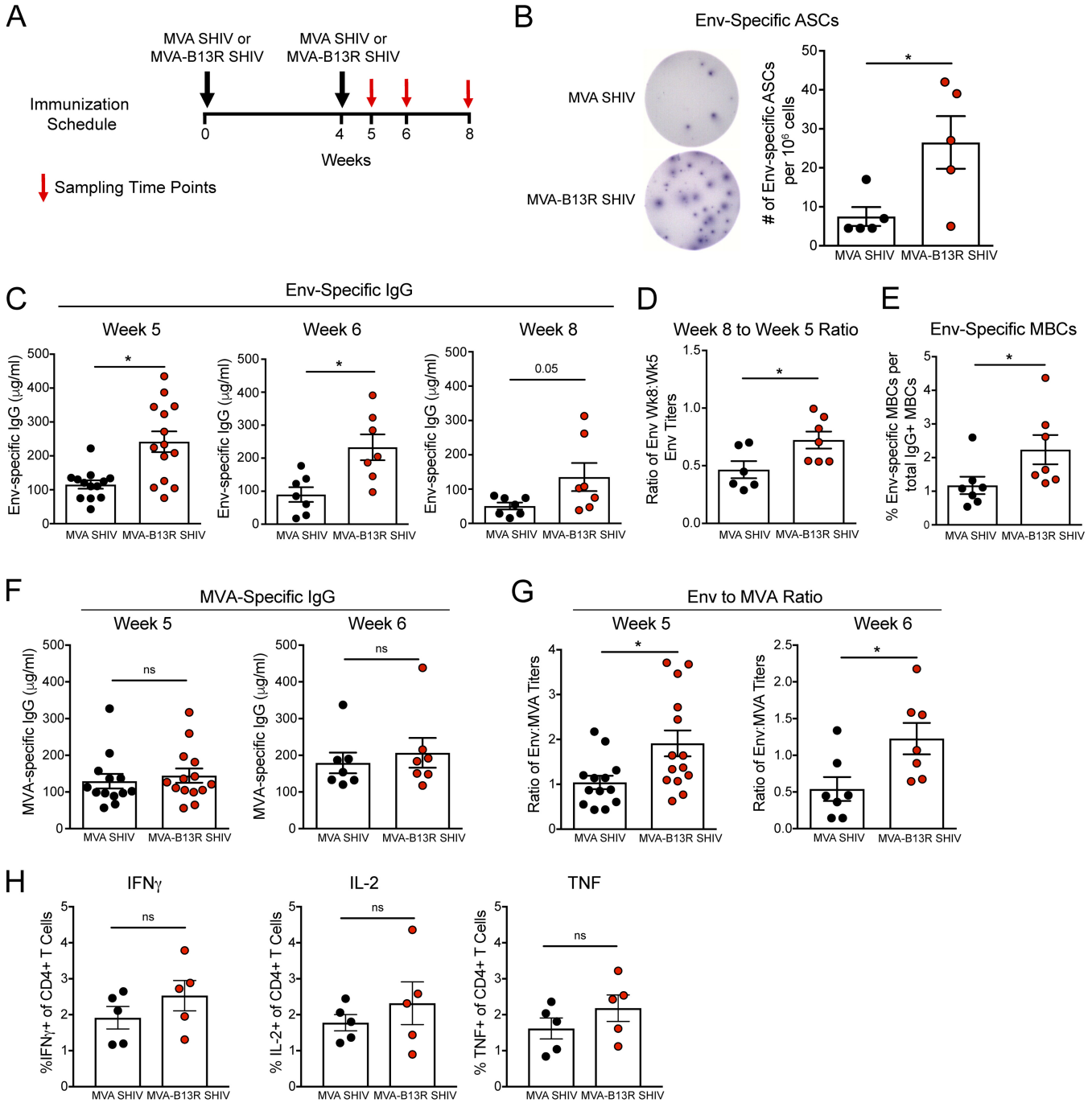

FIG 4 MVA-*B13R*/SHIV immunization enhances Env-specific humoral responses. BALB/c mice were immunized intramuscularly twice with 10^7 PFU/dose of MVA/SHIV or MVA-*B13R*/SHIV. (A) Schematic of the prime/boost immunization schedule and sampling time points. (B) Left, representative ELISpot of Env-specific IgG antibody-secreting cells (ASCs) at week 5 from MVA/SHIV- or MVA-*B13R*/SHIV-immunized mice. Right, Env-specific IgG ASCs measured from splenocytes at week 5. (C) Env-specific serum IgG titers were measured at weeks 5, 6, and 8. (D) Week 8-to-week 5 ratio of Env-specific serum IgG titers. (E) Env-specific memory B cells (MBCs) measured from splenocytes at week 8. (F) MVA-specific serum IgG titers measured at weeks 5 and 6. (G) Ratios of Env-specific to MVA-specific serum IgG titers at weeks 5 and 6. (H) Frequencies of HIV Env-specific and SIV Gag-specific IFN-γ–, IL-2-, and TNF-producing $CD4^+$ T cells from splenocytes at week 5. Bars represent mean values ± SEM. Data are representative of two or more independent experiments. Exact *P* values are reported for some data; *, $P < 0.05$; ns, not significant.

of Env-specific to MVA-specific serum IgG titers, MVA-*B13R*/SHIV-immunized mice had a higher ratio, which indicated skewing of humoral responses to the recombinant antigen of interest in comparison to the response to the viral vector backbone itself (Fig. 4G). Together, our results demonstrate the ability of our MVA-*B13R*/SHIV construct

to generate more antigen-specific humoral responses while avoiding the generation of excessive antivector responses. We also determined the SHIV-specific cellular responses to autologous HIV Env and SIV Gag antigens by stimulating with peptide pools for cytokine detection by intracellular cytokine staining (ICS) and enzyme-linked immunosorbent spot assay (ELISpot). These analyses did not reveal significant differences between the groups at week 5, demonstrating that MVA-*B13R*/SHIV did not enhance the T cell response (Fig. 4H).

MVA-*B13R*/SHIV delays antiviral IFN responses. In an effort to understand if there are any differences between MVA and MVA-*B13R* on a global level early after vaccination, we performed transcriptome sequencing (RNA-Seq) analysis. We immunized mice intramuscularly with 10^7 PFU of virus, and cells from the draining inguinal lymph nodes were isolated at 1, 2, and 6 days after immunization for RNA-Seq analysis. Inguinal lymph nodes were isolated from naive mice as a control. Differentially expressed genes (DEGs) between groups were defined as having a $\log_2$-fold change of >1.0 or <-1.0 and an adjusted *P* value of <0.05. For MVA/SHIV-immunized mice compared to naive mice, the number of DEGs peaked at day 1 with 255 DEGs and then decreased at days 2 and 6 (Fig. 5A). Metacore was used to curate a list of the top 50 enriched gene ontology (GO) processes for DEGs on each day, and subsequently, REViGO was used to summarize and display the GO processes in the form of a network (42). Analysis of the GO processes related to day 1 DEGs highlighted processes mainly related to type I and type II IFN responses, antiviral defense responses, and antigen processing and presentation (Fig. 5B). Analysis of day 2 samples from MVA/SHIV-immunized mice indicated mostly type I IFN responses, antiviral defense responses, and responses to compounds like corticosterone, cyclic AMP (cAMP), and calcium ion. The responses to molecules considered to be components of signaling cascades indicate a heightening of the global immune response at this point (Fig. 5C). At day 6, we observed a shift from innate immune responses to more adaptive immune responses, which included B cell activation, leukocyte differentiation, and antigen processing and presentation (Fig. 5D).

The number of DEGs detected in the comparison of MVA-*B13R*/SHIV-immunized and naive mice began with 66 DEGs at day 1, then increased to 226 at day 2 and 318 at day 6 (Fig. 5A). The different number of DEGs detected on each day for each vaccination group compared to naive mice indicated the potential differences in the early response generated by both viruses, particularly at day 1 after vaccination. Comparison of MVA-*B13R*/SHIV-immunized mice versus MVA/SHIV-immunized mice at day 1 did not yield DEGs, but there were 45 genes that had an adjusted *P* value of <0.05 regardless of $\log_2$-fold-change values, and select genes are depicted here (Fig. 5E). These genes are related to antiviral response (*Bst2*, *Ifi35*, *Nmi*, *Lgals9*, and *Samhd1*), antigen processing and presentation (*Psme2* and *Psmb9*), and apoptosis (*Casp8* and *Sp110*). Interestingly, 80% of the genes (36 of 45) have lower levels of expression in the MVA-*B13R*/SHIV-immunized group than in the MVA/SHIV-immunized group (data not shown).

Gene set enrichment analysis (GSEA) was performed to determine gene sets that were differentially enriched between groups. Gene sets with false discovery rates of <0.05 and normalized enrichment scores of >1.35 or <-1.35 were considered significantly enriched. GSEA results for day 1 samples from MVA/SHIV-immunized mice compared to samples from naive mice demonstrated enrichment in the IFN Alpha Response gene set, supporting the enhanced type I IFN responses detected in the GO process analysis (Fig. 5F, gray). Day 1 samples from MVA-*B13R*/SHIV-immunized mice also demonstrated enrichment for IFN-α responses compared to the results for samples from naive mice (Fig. 5F, red).

Surprisingly, when we performed GSEA comparisons of MVA-*B13R*/SHIV-immunized mice and MVA/SHIV-immunized mice at day 1 of vaccination, the MVA-*B13R*/SHIV-immunized group was negatively enriched for IFN-α responses compared to the MVA/SHIV-immunized mice, indicating that MVA-*B13R*/SHIV-immunized mice were mounting an IFN-α response to a lesser degree than MVA/SHIV-immunized mice (Fig. 5G). From the three GSEA comparisons performed (MVA/SHIV-immunized versus naive

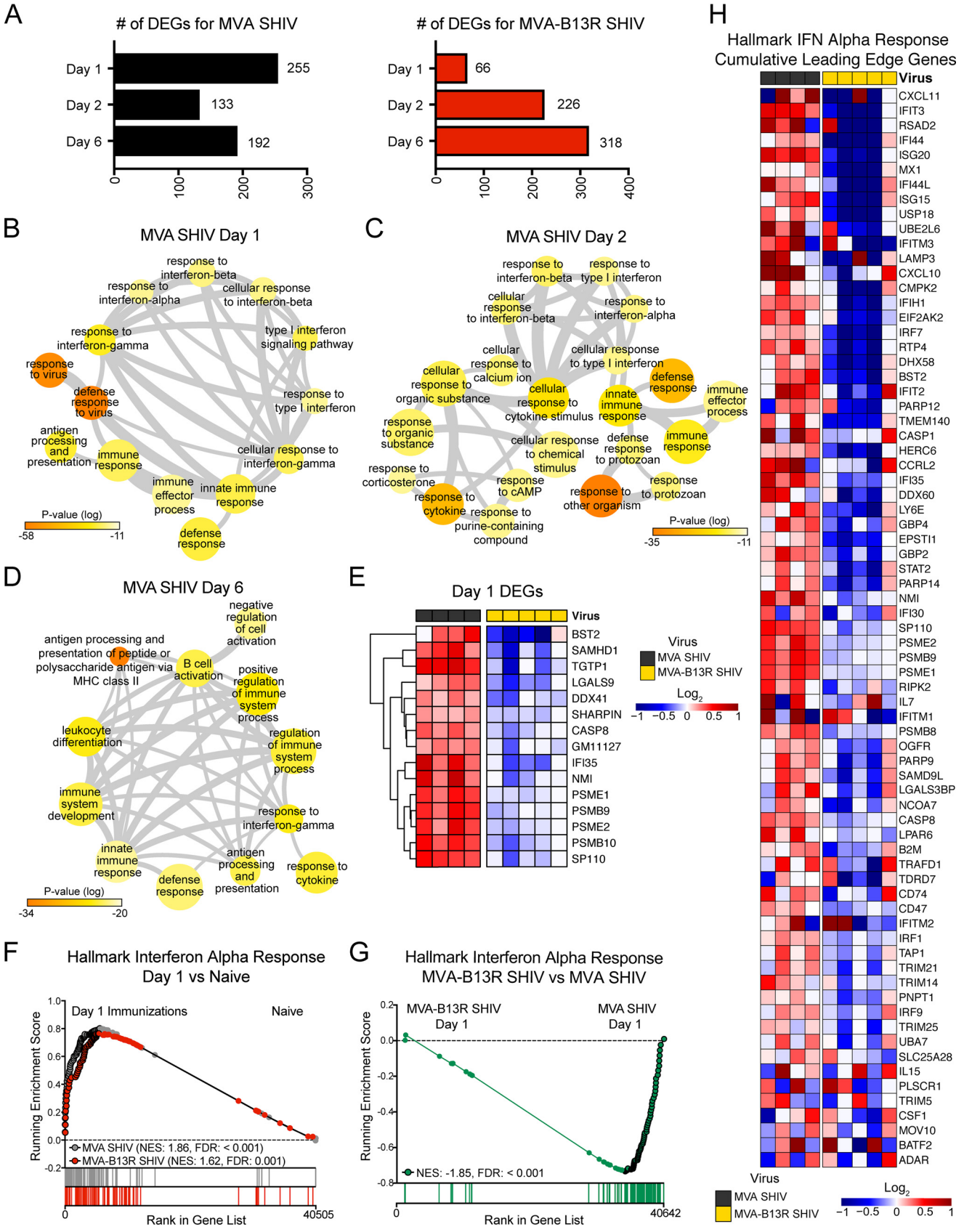

FIG 5 MVA-*B13R*/SHIV induces less robust type I and II interferon responses than MVA/SHIV. BALB/c mice were immunized intramuscularly with 10^7 PFU of MVA/SHIV or MVA-*B13R*/SHIV, and draining inguinal lymph node cells were isolated at days 1, 2, and 6 after immunization (n = 5/group/time point) for

(Continued on next page)

mice, MVA-*B13R*/SHIV-immunized versus naive mice, and MVA-*B13R*/SHIV- versus MVA/SHIV-immunized mice) with the Hallmark IFN Alpha Response gene set, we compiled a cumulative list of leading-edge genes and depicted the values from individual animals in a heatmap (43). We were able to observe that the MVA/SHIV-immunized group had higher expression levels of IFN-α signaling-related genes than the MVA-*B13R*/SHIV-immunized group (Fig. 5H). This pattern of lower expression levels in the MVA-*B13R*/SHIV-immunized group at day 1 was also seen for the Hallmark IFN Gamma Response gene set (data not shown). GSEA comparisons between both groups at days 2 and 6 resulted in no differences in responses, indicating that MVA-*B13R*/SHIV-immunized mice had delayed antiviral responses that became comparable by day 2 (data not shown). The data indicate that while both immunizations induced *in vivo* antiviral immune responses, MVA-*B13R*/SHIV-immunized mice were generating a less robust type I and II IFN response within the first day of immunization, which could influence the subsequent adaptive response.

DISCUSSION

Genetic modulation of poxviruses in order to create vectors that are both safe and immunogenic has been extensively studied and reviewed elsewhere (44–46). Here, we introduced a functional copy of the anti-apoptosis gene *B13R* from the WR strain of vaccinia virus into MVA. The expression of *B13R* during MVA infection demonstrated delayed cell death *in vitro* in muscle cells and professional APCs and improved the magnitude and durability of Env-specific antibody titers and memory B cell responses *in vivo*. Interestingly, MVA-*B13R*/SHIV immunizations were associated with negative enrichment of both type I and II IFN responses at 1 day after the priming vaccination compared to the IFN responses in the MVA/SHIV-immunized group. Collectively, these data show that restoring the function of the *181R*/*182R* genes using WR *B13R* in MVA significantly delays apoptosis of MVA-infected cells and that this is associated with enhanced humoral immunity and altered IFN signaling.

The immune mechanisms that led to enhanced humoral immunity need further investigation. The delay observed in apoptosis after infection with MVA-*B13R in vitro*, along with the concomitant increase in necrosis, may have been sufficient to influence the microenvironment and enhance the humoral response. Necrosis is a form of regulated cell death that can manifest in a variety of ways, including necroptosis and pyroptosis (47, 48). These forms of regulated necrosis are morphologically associated with cell swelling, mild chromatin condensation but with nuclei remaining intact, and the rapid loss of membrane integrity, leading to the release into the microenvironment of cellular contents such as damage-associated molecular patterns (DAMPs), which alert the immune system (49). The delayed apoptosis potentially allowed for a prolonged period of time when Env-loaded apoptotic bodies were being released and phagocytosed by APCs. Additionally, the combination of DAMPs and antigen directly released into the microenvironment due to necrosis could have influenced the humoral response. Tam et al. demonstrated that the administration of exponentially increasing doses of antigen over 1 week generated greater antibody titers than a single bolus administration and that the longer the period of time the increasing doses were administered over, the greater the antibody response (50). The relatively greater amounts of Env detected in cell lysates and supernatants through 96 h of infection by

FIG 5 Legend (Continued)
RNA-Seq analysis. Lymph nodes from naive mice ($n = 5$) were isolated as controls. One sample (MVA/SHIV mouse, day 1) was not included in the analysis as it mapped poorly to the reference sequence. (A) DEG analysis comparing mice at day 1, 2, or 6 after immunization to naive mice. DEG criteria were $\log_2$-fold change of >1.0 or <-1.0 and adjusted *P* value of <0.05. (B to D) Enriched gene ontology (GO) processes associated with DEGs from MVA/SHIV-immunized versus naive mice at day 1 (B), day 2 (C), and day 6 (D) were curated and visualized as a network. Colors are related to GO process *P* values, node sizes are related to numbers of related processes, and edge widths are related to degrees of similarity. (E) Heatmap depicting select DEGs from MVA/SHIV- compared to MVA-*B13R*/SHIV-immunized mice at day 1 after immunization. DEG criterion was an adjusted *P* value of <0.05. (F) Overlaid GSEAs comparing MVA/SHIV-immunized mice at day 1 to naive mice (gray) and MVA-*B13R*/SHIV-immunized mice at day 1 to naive mice (red). (G) GSEA comparing MVA-*B13R*/SHIV- to MVA/SHIV-immunized mice at day 1 after vaccination. (H) Heatmap of cumulative leading-edge genes from GSEAs shown in panels F and G. Heatmap colors represent the $\log_2$-fold-change values relative to the median value for each gene. NES, normalized enrichment score; FDR, false discovery rate. Leading-edge genes are shown as black-outlined dots.

MVA-*B13R*/SHIV indicate its potential to sustain Env production and release for a longer period of time than MVA/SHIV, which could have contributed to the improved humoral response (Fig. 3D).

Previously, Perdiguero et al. modulated MVA-induced apoptosis by deleting the anti-apoptotic *F1L* gene in MVA, which led to increased apoptosis and production of type I IFNs from infected cells (22). Immunizations with the *F1L* deletion mutant resulted in enhanced T cell responses, mainly directed at the Pol antigen, while gp120-specific antibody responses were not significantly different than the responses to immunizations with the parental MVA strain. Our approach of delaying apoptosis instead led to enhancement in antigen-specific humoral but not cellular responses. A possible difference between our *B13R*-expressing MVA and the *F1L* deletion MVA mutant may be the cytokines induced after infection. The MVA with *F1L* deleted enhanced the production of the type I IFN response *in vitro*. This is in contrast to delayed IFN responses observed with our MVA-*B13R*/SHIV construct in mice, which could contribute to differential intracellular signaling between the two vectors. Additionally, *F1L* has been described as a suppressor of the proapoptotic Bcl-2 family proteins and an inhibitor of caspase 9, the initiator caspase for the intrinsic apoptotic pathway (51–53), while *B13R* and its orthologs alternatively have been described as inhibitors of the extrinsic pathway (32, 33). The potential differences in IFN production and the targeting of different points of the apoptotic pathway may explain the differences in the adaptive immune responses observed.

Dai et al. showed that the detection of MVA in conventional DCs in mice is mediated by the cytosolic DNA sensor cyclic GMP-AMP synthase (cGAS), which signals through the adaptor protein STING and leads to induction of type I IFNs (54). They also indicated that processing of MVA virions after viral entry in the late endosomal and lysosomal compartments would lead to release of viral DNA into the cytoplasm, allowing detection by cGAS. Our RNA-Seq results from day 1 after immunization indicate that MVA-*B13R*/SHIV-vaccinated mice have significantly lower levels of expression of genes related to immunoproteasome assembly and antigen processing than MVA/SHIV-vaccinated mice, which is not observed at subsequent time points after immunization (Fig. 5E). Together, these observations indicate the possibility that MVA-*B13R* is influencing the lysosomal-processing pathway of a cell early during infection, hindering the release of viral DNA into the cytoplasm for detection by cGAS, and thereby delaying type I IFN production. STING has also been shown to be an adaptor protein for other cytosolic DNA sensors, such as DDX41 (55), which we observed to be expressed at a lower level at day 1 of MVA-*B13R*/SHIV immunizations, supporting our hypothesis of delayed viral DNA sensing (Fig. 5E). The decreased cell death we observed for MVA-*B13R*-infected pDCs and $CD141^+$ DCs supports the idea of slower viral sensing and cell death during MVA-*B13R* infection (Fig. 2G). The delay in cell death and viral sensing with MVA-*B13R*, in addition to the extended period of time when more antigen could be produced, likely is sufficient to influence the adaptive response.

Interestingly, among the DEGs observed at day 1 for MVA-*B13R*/SHIV- versus MVA/SHIV-immunized groups, *Casp8*, encoding caspase 8, was observed to be more highly expressed in the MVA/SHIV-immunized group than in the MVA-*B13R*/SHIV-immunized group (Fig. 5E). Caspase 8 is an initiator caspase of the apoptosis cascade that responds to extracellular stimuli for cell death, such as TNF-α or Fas ligand signaling (56). Caspase 8 activation leads to the initiation of downstream effector caspases, such as caspases 3, 6, and 7. The increased expression of *Casp8* in MVA/SHIV-immunized mice at 1 day after immunization may indicate an enhanced antiviral state among the cells of the draining lymph node that are likely responding to the inflammatory microenvironment and the presence of virus. The reduced expression of *Casp8* for the MVA-*B13R*/SHIV-immunized group suggests an association with the ability of MVA-*B13R* to inhibit caspase 8 activation and create a temporarily less inflammatory environment during the early stages of vaccination. It is possible that time points earlier than 24 h after immunization could have revealed further differences between the antiviral states induced by our two MVA vectors.

Others have shown the adjuvating properties of type I IFN signaling on humoral responses following acute infection or vaccination (57–60). We showed here that both MVA/SHIV and MVA-*B13R*/SHIV vaccinations induced significant IFN-α and IFN-γ responses compared to the levels in naive mice, as expected during an antiviral response; however, MVA-*B13R*/SHIV administration led to reduced expression levels for IFN signaling genes compared to MVA/SHIV at the early stages of infection, which became comparable by day 2 (Fig. 5F to H and data not shown). The data indicate that there is not an absence of IFN response occurring at this time, but there may be a slower ramping up to the peak of the immune response against MVA-*B13R*/SHIV, which could be due to less overall cell death occurring initially, delayed viral sensing by infected cells, and greater antigen production for an extended period of time. Altogether, these processes occurring early in the response may have influenced the enhanced Env-specific antibody and memory B cell levels we observed. Future studies to elucidate the differing early responses against these viruses *in vivo* are still required.

In summary, we show that MVA expressing an anti-apoptotic gene, *B13R*, is effective at delaying cell death of infected cells and capable of generating strong and durable Env-specific antibody titers and memory B cells when used as a vaccine vector (MVA-*B13R*/SHIV) in mice. These *in vivo* results are likely due to the increase in antigen levels produced over time, in addition to the delay of the antiviral inflammatory response generated against MVA-*B13R*. Studies in nonhuman primate (NHP) models would be informative to further determine the immunogenicity of the MVA-*B13R* vector, as the NHPs are closer to humans and will better inform the clinical utility of MVA-*B13R* as a vaccine vector.

MATERIALS AND METHODS

Generation of MVA-*B13R*. Due to high sequence homology between WR vaccinia virus *B13R* and MVA *181R*/*182R* genes (98.6% homology), we first knocked out MVA *181R*/*182R* from the genome via homologous recombination with PCR product 1, encoding the end of the MVA *180R* gene and the intergenic region at the end of *180R* (fragment A), a GFP-encoding cassette with a P11 promoter (fragment B), and the intergenic region at the start of MVA *183R* plus the beginning of the MVA *183R* gene (fragment C). Fragments A, B, and C were generated separately and designed to have at least 15 bp of overhang, which allowed the fragments to be assembled by overlap extension PCR. Fragment A was amplified from MVA DNA using forward primer LW-540 (5′-GGATATTGCATGATAGAATGGTTCGGTGG-3′) and reverse primer LW-541 (5′-AGAAGATATCCATAGTAATCGATATTGGTCG-3′). Fragment B was amplified from the plasmid insertion vector pLAS-1 using forward primer LW-542 (5′-CCAATATCGATTACTATGGA TATCTTCTTTTCATTTTGTTTTTTTCTATGCTATAAATGGTGAGCAAGG-3′) and reverse primer LW-543 (5′-TTA CTTGTACAGCTCGTGCATGCCG-3′). Fragment C was amplified from MVA DNA using forward primer LW-544 (5′-GGCATGCACGAGCTGTACAAGTAACCATTTTTTTTAAAAAAATAGAAAAAACATGTGGTATTAG TGC-3′) and reverse primer LW-545 (5′-CACAATCTTTGACATCATCCCACGGC-3′). For overlap extension PCR of fragments A, B, and C, forward primer LW-540 and reverse primer LW-545 were used. Following recombination of the GFP-encoding PCR product into MVA and plaque purification, the GFP-encoding sequence was subsequently knocked out with PCR product 2, encoding WR *B13R* flanked by fragments A and C as described above via recombination. PCR product 2 was amplified from WR DNA using forward primer LW-540 and reverse primer LW-545 (the same primers can be used due to the presence of identical sequences in the MVA and WR genomes). Recombinants were plaque purified to generate MVA-*B13R*. Sequences were confirmed for both PCR products and MVA-*B13R* viruses (GenBank accession number MK170380). Lysates of virus-infected DF-1 cells were purified through a 36% sucrose cushion for virus stocks.

***In vitro* infections.** DF-1 cells (spontaneously immortalized chicken embryo fibroblast cell line), HeLa cells, C2C12 cells (a mouse myoblast cell line [CRL-1772; ATCC]), and RD cells (a human muscle rhabdomyosarcoma cell line [CCL-136; ATCC]) were cultured in Dulbecco's modified Eagle's medium (DMEM) supplemented with 10% fetal bovine serum (FBS), 100 units penicillin/ml, 0.1 mg/ml streptomycin, and 1% L-glutamine. For infections, MVA viruses at the MOIs indicated in the relevant figure legends were added in complete DMEM with 2% FBS. After 1.5 to 2 h of inoculation, the inoculum was removed and fresh 10% FBS– complete DMEM was added. To harvest cells, DMEM was removed, and cells were washed with warm phosphate-buffered saline (PBS) and treated with trypsin to release cells into suspension. For testing the effect of various caspase inhibitors during MVA infection, individual caspase inhibitors (R&D Systems) were reconstituted in dimethyl sulfoxide (DMSO). Cells were inoculated with virus at an MOI of 2 for 2 h. The inoculum was replaced with fresh complete DMEM containing 100 μM of the individual caspase inhibitors, and cells were harvested 48 h postinfection to be stained for intracellular active caspase 3 expression. For testing the functionality of *B13R* during MVA infection, HeLa cells were inoculated with virus at an MOI of 3 for 1.5 to 2 h, the inoculum was removed, and fresh DMEM was added. Sixteen hours later, the medium was replaced with DMEM containing 25 ng/ml recombinant

human TNF-α (Tonbo) and 5 μg/ml cycloheximide (Sigma), and cells were harvested for staining at various time points posttreatment.

Western blot analysis. DF-1 cells were infected at the MOIs of virus indicated in the relevant figure legends and harvested at various time points postinfection. Supernatant was collected and centrifuged to ensure separation of cells. After infected cells were washed with cold PBS, RIPA buffer (ThermoScientific) with protease inhibitor was added and cell lysates were collected according to the manufacturer's protocol. Lysate or supernatant samples were added to Laemmli buffer containing β-mercaptoethanol, heated to 95°C, and run on 4 to 15% SDS-PAGE gels for Western blotting. *B13R* was detected with polyclonal rabbit anti-*B13R* antiserum (diluted 1:5,000; gift from Geoffrey Smith, University of Cambridge), Gag was detected with a mouse anti-Gag p27 monoclonal antibody (2F12; NIH AIDS Reagent Program), and Env was detected with a mouse anti-Env monoclonal antibody (ID6; NIH AIDS Reagent Program). Secondary goat anti-rabbit Ig-horseradish peroxidase (HRP) (diluted 1:5,000; Southern Biotech) or goat anti-mouse IgG-HRP (diluted 1:10,000; Southern Biotech) was used for detection. Enhanced chemiluminescence (ECL) substrate (GE Healthcare) was used for chemiluminescence detection. Image Lab version 6 (Bio-Rad) was used for densitometry analysis.

Analysis of virus growth. DF-1 cells were infected at an MOI of 0.05 with MVA or MVA-*B13R*. At indicated time points postinfection, cell layers were washed with PBS and trypsinized to harvest cells. Collected cells were freeze-thawed at −80°C/37°C, respectively, and sonicated three times to ensure disruption of cell membranes and release of virus. Titers of virus recovered from lysates were determined on DF-1 cells by plaque assay.

Infection of rhesus macaque PBMCs. For *ex vivo* infection of rhesus macaque peripheral blood mononuclear cells (PBMCs), blood was collected from naive rhesus macaques in sodium citrate CPT tubes. Samples were centrifuged at 2,800 rpm for 30 min at room temperature with no deceleration. Buffy coats containing PBMCs were collected, washed with Hanks balanced salt solution (HBSS) without calcium and magnesium, and resuspended in complete RPMI medium (RPMI, 10% FBS, 100 units penicillin/ml, 0.1 mg/ml streptomycin, 10 μM HEPES). Isolated PBMCs were infected with virus at an MOI of 3 for 20 h at 37°C and then stained for MVA, cell subset markers, and viability markers for flow cytometry analysis.

Generation of recombinant MVAs expressing SHIV antigens. All recombinant SHIV-expressing MVA vectors expressed the SIVmac239 Gag and Pol genes under an independent early/late vaccinia virus promoter (modified H5 [mH5]) recombined into the deletion III site of MVA. The modified clade C HIV Env 1086C gp150 K160N gene (GenBank accession number FJ444399.1) (61) was cloned between two XmaI restriction sites of the plasmid transfer vector pLW-73 and used to recombine into the essential region of the MVA genome (between genes *I8R* and *G1L*) under an independent mH5 promoter. Recombinant MVAs were plaque purified and tested for contamination with parental MVAs by PCR using primers in the deletion III flanking regions. Lysates of virus-infected DF-1 cells were purified through a 36% sucrose cushion for virus stocks.

Flow cytometry. For *in vitro* detection of cells undergoing cell death, virally infected cells were harvested and stained with LIVE/DEAD cell viability stain (ThermoFisher), fixed and permeabilized with Cytofix/Cytoperm (BD Biosciences), and stained intracellularly for MVA E3 protein (TW2.3; BEI Resources) and active caspase 3 (C92-605; BD Pharmingen). For detecting the expression of SIV Gag and HIV Env by SHIV constructs, virally infected cells were stained with LIVE/DEAD cell viability stain, fixed and permeabilized with Cytofix/Cytoperm, and stained intracellularly with monoclonal antibodies to p27 Gag (2F12; NIH AIDS Reagent Program) and HIV Env (ID6; NIH AIDS Reagent Program). Infected rhesus macaque PBMCs were surface stained with the following: LIVE/DEAD near-IR cell viability stain and anti-CD3 (SP-34-2; BD Biosciences), anti-CD14 (M5E2; BioLegend), anti-CD11c (3.9; BioLegend), anti-CD123 (6H6; BioLegend), anti-CD20 (2H7; BioLegend), anti-CD16 (3G8; Sony Biotechnology), anti-HLA-DR (G46-6; BD Biosciences), and anti-CD141 (1A4; BD Biosciences) antibodies. Cells were fixed and permeabilized with Cytofix/Cytoperm and stained intracellularly for active caspase 3 and MVA. Cells were acquired on an LSR Fortessa instrument and analyzed using FlowJo software (Tree Star, Inc.). For intracellular cytokine staining, stimulated mouse splenocytes were stained with LIVE/DEAD cell viability stain and anti-CD4 (RM4-5; Tonbo) and anti-CD8 (53-6.7; BioLegend) antibodies. Cells were then fixed and permeabilized with Cytofix/Cytoperm and stained intracellularly for IFN-γ (XMG1.2; BD Biosciences), IL-2 (JES6-5H4; BD Biosciences), and TNF (MP6-XT22; BD Biosciences).

Mice, immunizations, and sample collection. Six- to 8-week-old female BALB/c mice were purchased from Charles River Laboratory. For MVA immunizations, mice were intramuscularly immunized with 10^7 PFU of virus diluted in sterile PBS. After immunization, blood was collected via tail-vein bleed and serum was isolated and stored at −20°C. Where applicable, cells were isolated from spleens and inguinal lymph nodes by manual disruption through 100 μM strainers in complete RPMI medium (RPMI, 10% FBS, 100 units penicillin/ml, 0.1 mg/ml streptomycin, 10 μM HEPES, and 55 μM β-mercaptoethanol). Red blood cells were lysed with ammonium-chloride-potassium (ACK) lysing buffer and washed twice with PBS at 1,200 rpm for 10 min prior to use.

Measuring antibody titers. For enzyme-linked immunosorbent assays (ELISAs), plates were coated with 0.5 μg/ml recombinant HIV gp140 (C.1086 gp140C K160N; NIH AIDS Reagent Program) or 10^7 PFU/ml MVA diluted in 0.2 M bicarbonate buffer, pH 9.4. A concentration of 2.0 μg/ml goat anti-mouse IgG (M2650; Sigma) was used to coat wells for standards. Plates were blocked for 1 h at room temperature with 5% nonfat dry milk and 4% whey in PBS with 0.05% Tween 20 (PBS-T). Serum samples and standard dilutions were prepared in 4% whey in PBS-T. Purified mouse IgG (0107-01; Southern Biotech) was used as the IgG standard. Samples or standards were incubated for 2 h at room temperature, and plates were washed six times with PBS-T. Bound Env-specific IgG was detected

using goat anti-mouse IgG-HRP (1030-05; Southern Biotech) at 1:40,000 dilution for 1 h at room temperature, and then wells were developed using TMB (3,3′,5,5′-tetramethylbenzidine) peroxidase substrate (KPL).

ELISpot assays. For antibody-secreting cells, 96-well ELISpot plates (Millipore) were coated with 0.5 μg/ml gp140 or 1.0 μg/ml goat anti-mouse Ig (Southern Biotech) in PBS overnight at 4°C. Plates were washed six times with PBS-T and three times with PBS and then blocked with complete RPMI medium for at least 2 h at 37°C. Cells were resuspended in complete RPMI medium, and a series of 1:2 or 1:3 dilutions of cells were added to plates and the plates incubated for 5 h at 37°C. Goat anti-mouse IgG biotin (Southern Biotech) diluted in PBS-T with 1.0% serum was added for 1 h at room temperature to detect bound mouse IgG antibody. Streptavidin-alkaline phosphatase (Mabtech) diluted in PBS-T with 1.0% serum was added for 1 h at room temperature in the dark, followed by 1-Step nitro-blue tetrazolium (NBT) substrate (ThermoScientific) to detect spots. For memory B cell assays, 10^6 isolated splenocytes were cultured in flat-bottom 24-well plates and stimulated with 1 μg/ml resiquimod (Sigma) and 10 ng/ml recombinant murine IL-2 (Peprotech) in complete RPMI medium in replicates of 8 or left unstimulated in the medium. Cells were incubated for 3 days at 37°C. ELISpot plates were prepared as described above. Stimulated cells were washed twice with PBS and resuspended in fresh complete RPMI medium. Cells for each replicate were diluted accordingly and divided for plating for detection of either antigen-specific or total IgG antibody production. Cells were incubated on plates for 5 h at 37°C. Secondary and detection antibody procedures for antibody-secreting cell assays were the same as described above.

Intracellular cytokine stimulations. Amounts of 10^6 splenocytes were cultured in 200 μl complete RPMI medium (RPMI, 10% FBS, 100 units penicillin/ml, 0.1 mg/ml streptomycin, 10 μM HEPES, and 55 μM β-mercaptoethanol) with HIV Env 1086C peptides or SIVmac239 Gag peptides at 37°C. After 1.5 h, GolgiStop (BD Biosciences) and brefeldin A (Sigma) were added to each sample and the mixtures cultured for an additional 4.5 h, followed by antibody staining for flow cytometry.

RNA-Seq. RNA-Seq analyses were conducted at the Yerkes NHP Genomics Core on naive (n = 5), MVA/SHIV-immunized (n = 5/time point at 3 time points), and MVA-*B13R*/SHIV-immunized (n = 5/time point at 3 time points) mice. RNA was extracted from lymph node cells in Qiagen buffer RLT by using the Qiagen RNeasy micro protocol as described previously (62) and assessed for integrity and quantity using an Agilent Bioanalyzer (Agilent Technologies, Santa Clara, CA). An amount of 2 ng of total RNA was used as input for mRNA amplification using 5′ template-switch PCR with the SMART-Seq version 4 ultralow input RNA kit (TaKaRa Bio USA, Inc.) according to the manufacturer's instructions. Amplified mRNA was fragmented and appended with dual indexed bar codes using Illumina NexteraXT DNA library prep kits. Amplified libraries were validated using the Agilent 4200 TapeStation and quantified using a Qubit fluorometer. Libraries were normalized and pooled, followed by clustering on a HiSeq 3000/HiSeq 4000 flow cell using the Illumina cBot system. The clustered flow cell was then sequenced on the Illumina HiSeq 3000 system, employing a single-end 101-cycle run with multiplexing to achieve approximately 20 million reads per sample.

RNA-Seq statistical analyses. RNA-Seq data were aligned to the GRCm38.p3 assembly of the mouse genome from GENCODE (available at ftp://ftp.ebi.ac.uk/pub/databases/gencode/Gencode_mouse/release_M3/). Alignment was performed using STAR version 2.5.2b. Transcript abundance was estimated internally with STAR using the htseq-count algorithm. One sample (MVA/SHIV-immunized mouse, day 1) was discontinued from further analysis as it mapped poorly to the reference sequence. Differential expression analyses were performed between two sample sets using DESeq2 (significance was set at an adjusted P value of <0.05 and $\log_2$-fold change of >1.0 or <-1.0). Genes with a total count of less than 20 counts across all samples (total n = 35) were excluded from analysis. DEGs from a comparison were analyzed through Metacore from Thomson Reuters for the top 50 enriched gene ontology (GO) processes. REViGO (http://revigo.irb.hr/) and Cytoscape software were used to visualize related enriched GO processes with nodes and links with similar terms linked with edges (42, 63). Color is related to the GO process P value, node size is related to the number of related processes, and edge width is related to the degree of similarity. The attribute values of each network are relative to the maximum and minimum values of that network. Gene set enrichment analysis (GSEA) was performed using the desktop module available from the Broad Institute (https://www.broadinstitute.org/gsea/). GSEA was run for MSigDB curated gene set collections with 1,000 permutations using the gene set permutation type (normalized enrichment score cutoff of >1.35 or <-1.35 and false discovery rate of <0.05). The chip platform used was derived from the GRCm38-p3 mouse reference used for mapping and abundance estimation.

Statistics. Statistical analysis was performed using repeated-measure two-way analysis of variance (ANOVA) with Tukey test to correct for multiple comparisons (when comparing two or more groups over various time points), two-tailed unpaired Mann-Whitney test (when comparing two groups), or two-tailed paired Student t test (when comparing matched samples) using Prism 7.0d (GraphPad) software. P values of <0.05 were considered statistically significant.

Study approval. Mice were maintained and used according to institutional and NIH guidelines in a specific-pathogen-free facility. All animal studies were approved by Emory University IACUC (Atlanta, GA).

Data availability. The RNA-Seq data set is available at the GEO repository under accession number GSE119884.

The data that support the findings of this study are available upon request from the corresponding author.

ACKNOWLEDGMENTS

We thank the veterinary staff at Yerkes for animal care, the Emory Electron Microscopy Core for imaging services, the CFAR Immunology Core for help with flow cytometry, and Nirav Patel at the Yerkes NHP Genomics Core for sample processing, library preparation, and sequencing. We thank Gregory Tharp and Lisa Mills for advice and helpful discussions regarding RNA-Seq analysis. We thank Koichi Araki for WR vaccinia virus-infected DF-1 cell lysate and Geoffrey Smith at the University of Cambridge for the gift of the rabbit anti-*B13R* antisera.

We declare that no conflicts of interest exist.

This work was supported in part by National Institutes of Health grants U19AI109633 and R01DE02633 (to R.R.A.), Emory University CFAR grant P30 AI050409, NCRR/NIH base grant P30 RR00165 (to YNPRC), and by funding from the Division of Intramural Research, NIAID, to B.M.

REFERENCES

1. Volz A, Sutter G. 2017. Modified vaccinia virus Ankara: history, value in basic research, and current perspectives for vaccine development. Adv Virus Res 97:187–243. https://doi.org/10.1016/bs.aivir.2016.07.001.
2. Smith GL, Moss B. 1983. Infectious poxvirus vectors have capacity for at least 25,000 base pairs of foreign DNA. Gene 25:21–28. https://doi.org/10.1016/0378-1119(83)90163-4.
3. Sutter G, Moss B. 1992. Nonreplicating vaccinia vector efficiently expresses recombinant genes. Proc Natl Acad Sci U S A 89:10847–10851. https://doi.org/10.1073/pnas.89.22.10847.
4. Baden LR, Walsh SR, Seaman MS, Cohen YZ, Johnson JA, Licona JH, Filter RD, Kleinjan JA, Gothing JA, Jennings J, Peter L, Nkolola J, Abbink P, Borducchi EN, Kirilova M, Stephenson KE, Pegu P, Eller MA, Trinh HV, Rao M, Ake JA, Sarnecki M, Nijs S, Callewaert K, Schuitemaker H, Hendriks J, Pau MG, Tomaka F, Korber BT, Alter G, Dolin R, Earl PL, Moss B, Michael NL, Robb ML, Barouch DH, IPCAVD006/RV380/HIV-V-A002 Study Group. 2018. First-in-human randomized controlled trial of mosaic HIV-1 immunogens delivered via a modified vaccinia Ankara vector. J Infect Dis 218:633–644. https://doi.org/10.1093/infdis/jiy212.
5. Njuguna IN, Ambler G, Reilly M, Ondondo B, Kanyugo M, Lohman-Payne B, Gichuhi C, Borthwick N, Black A, Mehedi SR, Sun J, Maleche-Obimbo E, Chohan B, John-Stewart GC, Jaoko W, Hanke T. 2014. PedVacc 002: a phase I/II randomized clinical trial of MVA.HIVA vaccine administered to infants born to human immunodeficiency virus type 1-positive mothers in Nairobi. Vaccine 32:5801–5808. https://doi.org/10.1016/j.vaccine.2014.08.034.
6. Currier JR, Ngauy V, de Souza MS, Ratto-Kim S, Cox JH, Polonis VR, Earl P, Moss B, Peel S, Slike B, Sriplienchan S, Thongcharoen P, Paris RM, Robb ML, Kim J, Michael NL, Marovich MA. 2010. Phase I safety and immunogenicity evaluation of MVA-CMDR, a multigenic, recombinant modified vaccinia Ankara-HIV-1 vaccine candidate. PLoS One 5:e13983. https://doi.org/10.1371/journal.pone.0013983.
7. Goepfert PA, Elizaga ML, Seaton K, Tomaras GD, Montefiori DC, Sato A, Hural J, DeRosa SC, Kalams SA, McElrath MJ, Keefer MC, Baden LR, Lama JR, Sanchez J, Mulligan MJ, Buchbinder SP, Hammer SM, Koblin BA, Pensiero M, Butler C, Moss B, Robinson HL, HVTN 205 Study Group, National Institutes of Allergy and Infectious Diseases HIV Vaccines Trials Network. 2014. Specificity and 6-month durability of immune responses induced by DNA and recombinant modified vaccinia Ankara vaccines expressing HIV-1 virus-like particles. J Infect Dis 210:99–110. https://doi.org/10.1093/infdis/jiu003.
8. Lai L, Kwa SF, Kozlowski PA, Montefiori DC, Nolen TL, Hudgens MG, Johnson WE, Ferrari G, Hirsch VM, Felber BK, Pavlakis GN, Earl PL, Moss B, Amara RR, Robinson HL. 2012. SIVmac239 MVA vaccine with and without a DNA prime, similar prevention of infection by a repeated dose SIVsmE660 challenge despite different immune responses. Vaccine 30:1737–1745. https://doi.org/10.1016/j.vaccine.2011.12.026.
9. La Rosa C, Longmate J, Martinez J, Zhou Q, Kaltcheva TI, Tsai W, Drake J, Carroll M, Wussow F, Chiuppesi F, Hardwick N, Dadwal S, Aldoss I, Nakamura R, Zaia JA, Diamond DJ. 2017. MVA vaccine encoding CMV antigens safely induces durable expansion of CMV-specific T cells in healthy adults. Blood 129:114–125. https://doi.org/10.1182/blood-2016-07-729756.
10. Domi A, Feldmann F, Basu R, McCurley N, Shifflett K, Emanuel J, Hellerstein MS, Guirakhoo F, Orlandi C, Flinko R, Lewis GK, Hanley PW, Feldmann H, Robinson HL, Marzi A. 2018. A single dose of modified vaccinia Ankara expressing Ebola virus like particles protects nonhuman primates from lethal Ebola virus challenge. Sci Rep 8:864. https://doi.org/10.1038/s41598-017-19041-y.
11. Lazaro-Frias A, Gomez-Medina S, Sanchez-Sampedro L, Ljungberg K, Ustav M, Liljestrom P, Munoz-Fontela C, Esteban M, Garcia-Arriaza J. 2018. Distinct immunogenicity and efficacy of poxvirus-based vaccine candidates against Ebola virus expressing GP and VP40 proteins. J Virol 92:e00363-18. https://doi.org/10.1128/JVI.00363-18.
12. Heery CR, Palena C, McMahon S, Donahue RN, Lepone LM, Grenga I, Dirmeier U, Cordes L, Marte J, Dahut W, Singh H, Madan RA, Fernando RI, Hamilton DH, Schlom J, Gulley JL. 2017. Phase I study of a poxviral TRICOM-based vaccine directed against the transcription factor brachyury. Clin Cancer Res 23:6833–6845. https://doi.org/10.1158/1078-0432.CCR-17-1087.
13. Taylor GS, Jia H, Harrington K, Lee LW, Turner J, Ladell K, Price DA, Tanday M, Matthews J, Roberts C, Edwards C, McGuigan L, Hartley A, Wilson S, Hui EP, Chan AT, Rickinson AB, Steven NM. 2014. A recombinant modified vaccinia Ankara vaccine encoding Epstein-Barr virus (EBV) target antigens: a phase I trial in UK patients with EBV-positive cancer. Clin Cancer Res 20:5009–5022. https://doi.org/10.1158/1078-0432.CCR-14-1122-T.
14. Kreijtz JH, Goeijenbier M, Moesker FM, van den Dries L, Goeijenbier S, De Gruyter HL, Lehmann MH, Mutsert G, van de Vijver DA, Volz A, Fouchier RA, van Gorp EC, Rimmelzwaan GF, Sutter G, Osterhaus AD. 2014. Safety and immunogenicity of a modified-vaccinia-virus-Ankara-based influenza A H5N1 vaccine: a randomised, double-blind phase 1/2a clinical trial. Lancet Infect Dis 14:1196–1207. https://doi.org/10.1016/S1473-3099(14)70963-6.
15. Hardwick NR, Carroll M, Kaltcheva T, Qian D, Lim D, Leong L, Chu P, Kim J, Chao J, Fakih M, Yen Y, Espenschied J, Ellenhorn JD, Diamond DJ, Chung V. 2014. p53MVA therapy in patients with refractory gastrointestinal malignancies elevates p53-specific CD8+ T-cell responses. Clin Cancer Res 20:4459–4470. https://doi.org/10.1158/1078-0432.CCR-13-3361.
16. Hui EP, Taylor GS, Jia H, Ma BB, Chan SL, Ho R, Wong WL, Wilson S, Johnson BF, Edwards C, Stocken DD, Rickinson AB, Steven NM, Chan AT. 2013. Phase I trial of recombinant modified vaccinia Ankara encoding Epstein-Barr viral tumor antigens in nasopharyngeal carcinoma patients. Cancer Res 73:1676–1688. https://doi.org/10.1158/0008-5472.CAN-12-2448.
17. Pathan AA, Minassian AM, Sander CR, Rowland R, Porter DW, Poulton ID, Hill AV, Fletcher HA, McShane H. 2012. Effect of vaccine dose on the safety and immunogenicity of a candidate TB vaccine, MVA85A, in BCG vaccinated UK adults. Vaccine 30:5616–5624. https://doi.org/10.1016/j.vaccine.2012.06.084.
18. Garber DA, O'Mara LA, Zhao J, Gangadhara S, An I, Feinberg MB. 2009. Expanding the repertoire of modified vaccinia Ankara-based vaccine vectors via genetic complementation strategies. PLoS One 4:e5445. https://doi.org/10.1371/journal.pone.0005445.

19. Garber DA, O'Mara LA, Gangadhara S, McQuoid M, Zhang X, Zheng R, Gill K, Verma M, Yu T, Johnson B, Li B, Derdeyn CA, Ibegbu C, Altman JD, Hunter E, Feinberg MB. 2012. Deletion of specific immune-modulatory genes from modified vaccinia virus Ankara-based HIV vaccines engenders improved immunogenicity in rhesus macaques. J Virol 86:12605–12615. https://doi.org/10.1128/JVI.00246-12.
20. Garcia-Arriaza J, Najera JL, Gomez CE, Tewabe N, Sorzano CO, Calandra T, Roger T, Esteban M. 2011. A candidate HIV/AIDS vaccine (MVA-B) lacking vaccinia virus gene C6L enhances memory HIV-1-specific T-cell responses. PLoS One 6:e24244. https://doi.org/10.1371/journal.pone.0024244.
21. Garcia-Arriaza J, Najera JL, Gomez CE, Sorzano CO, Esteban M. 2010. Immunogenic profiling in mice of a HIV/AIDS vaccine candidate (MVA-B) expressing four HIV-1 antigens and potentiation by specific gene deletions. PLoS One 5:e12395. https://doi.org/10.1371/journal.pone.0012395.
22. Perdiguero B, Gomez CE, Najera JL, Sorzano CO, Delaloye J, Gonzalez-Sanz R, Jimenez V, Roger T, Calandra T, Pantaleo G, Esteban M. 2012. Deletion of the viral anti-apoptotic gene F1L in the HIV/AIDS vaccine candidate MVA-C enhances immune responses against HIV-1 antigens. PLoS One 7:e48524. https://doi.org/10.1371/journal.pone.0048524.
23. Falivene J, Del Medico Zajac MP, Pascutti MF, Rodriguez AM, Maeto C, Perdiguero B, Gomez CE, Esteban M, Calamante G, Gherardi MM. 2012. Improving the MVA vaccine potential by deleting the viral gene coding for the IL-18 binding protein. PLoS One 7:e32220. https://doi.org/10.1371/journal.pone.0032220.
24. Garcia-Arriaza J, Gomez CE, Sorzano CO, Esteban M. 2014. Deletion of the vaccinia virus N2L gene encoding an inhibitor of IRF3 improves the immunogenicity of modified vaccinia virus Ankara expressing HIV-1 antigens. J Virol 88:3392–3410. https://doi.org/10.1128/JVI.02723-13.
25. Kerr JF, Wyllie AH, Currie AR. 1972. Apoptosis: a basic biological phenomenon with wide-ranging implications in tissue kinetics. Br J Cancer 26:239–257. https://doi.org/10.1038/bjc.1972.33.
26. Fadok VA, Bratton DL, Frasch SC, Warner ML, Henson PM. 1998. The role of phosphatidylserine in recognition of apoptotic cells by phagocytes. Cell Death Differ 5:551–562. https://doi.org/10.1038/sj.cdd.4400404.
27. Spel L, Boelens JJ, Nierkens S, Boes M. 2013. Antitumor immune responses mediated by dendritic cells: how signals derived from dying cancer cells drive antigen cross-presentation. Oncoimmunology 2:e26403. https://doi.org/10.4161/onci.26403.
28. Fang ZY, Limbach K, Tartaglia J, Hammonds J, Chen X, Spearman P. 2001. Expression of vaccinia E3L and K3L genes by a novel recombinant canarypox HIV vaccine vector enhances HIV-1 pseudovirion production and inhibits apoptosis in human cells. Virology 291:272–284. https://doi.org/10.1006/viro.2001.1209.
29. Sasaki S, Amara RR, Oran AE, Smith JM, Robinson HL. 2001. Apoptosis-mediated enhancement of DNA-raised immune responses by mutant caspases. Nat Biotechnol 19:543–547. https://doi.org/10.1038/89289.
30. Dobbelstein M, Shenk T. 1996. Protection against apoptosis by the vaccinia virus SPI-2 (B13R) gene product. J Virol 70:6479–6485.
31. Kettle S, Blake NW, Law KM, Smith GL. 1995. Vaccinia virus serpins B13R (SPI-2) and B22R (SPI-1) encode M(r) 38.5 and 40K, intracellular polypeptides that do not affect virus virulence in a murine intranasal model. Virology 206:136–147. https://doi.org/10.1016/S0042-6822(95)80028-X.
32. Kettle S, Alcamí A, Khanna A, Ehret R, Jassoy C, Smith GL. 1997. Vaccinia virus serpin B13R (SPI-2) inhibits interleukin-1beta-converting enzyme and protects virus-infected cells from TNF- and Fas-mediated apoptosis, but does not prevent IL-1beta-induced fever. J Gen Virol 78(Pt 3):677–685. https://doi.org/10.1099/0022-1317-78-3-677.
33. Zhou Q, Snipas S, Orth K, Muzio M, Dixit VM, Salvesen GS. 1997. Target protease specificity of the viral serpin CrmA. Analysis of five caspases. J Biol Chem 272:7797–7800. https://doi.org/10.1074/jbc.272.12.7797.
34. Quan LT, Caputo A, Bleackley RC, Pickup DJ, Salvesen GS. 1995. Granzyme B is inhibited by the cowpox virus serpin cytokine response modifier A. J Biol Chem 270:10377–10379. https://doi.org/10.1074/jbc.270.18.10377.
35. Antoine G, Scheiflinger F, Dorner F, Falkner FG. 1998. The complete genomic sequence of the modified vaccinia Ankara strain: comparison with other orthopoxviruses. Virology 244:365–396. https://doi.org/10.1006/viro.1998.9123.
36. Palucka K, Banchereau J, Mellman I. 2010. Designing vaccines based on biology of human dendritic cell subsets. Immunity 33:464–478. https://doi.org/10.1016/j.immuni.2010.10.007.
37. Karrich JJ, Jachimowski LC, Uittenbogaart CH, Blom B. 2014. The plasmacytoid dendritic cell as the Swiss army knife of the immune system: molecular regulation of its multifaceted functions. J Immunol 193:5772–5778. https://doi.org/10.4049/jimmunol.1401541.
38. Jongbloed SL, Kassianos AJ, McDonald KJ, Clark GJ, Ju X, Angel CE, Chen CJ, Dunbar PR, Wadley RB, Jeet V, Vulink AJ, Hart DN, Radford KJ. 2010. Human CD141+ (BDCA-3)+ dendritic cells (DCs) represent a unique myeloid DC subset that cross-presents necrotic cell antigens. J Exp Med 207:1247–1260. https://doi.org/10.1084/jem.20092140.
39. Meixlsperger S, Leung CS, Ramer PC, Pack M, Vanoaica LD, Breton G, Pascolo S, Salazar AM, Dzionek A, Schmitz J, Steinman RM, Munz C. 2013. CD141+ dendritic cells produce prominent amounts of IFN-alpha after dsRNA recognition and can be targeted via DEC-205 in humanized mice. Blood 121:5034–5044. https://doi.org/10.1182/blood-2012-12-473413.
40. Segura E, Valladeau-Guilemond J, Donnadieu MH, Sastre-Garau X, Soumelis V, Amigorena S. 2012. Characterization of resident and migratory dendritic cells in human lymph nodes. J Exp Med 209:653–660. https://doi.org/10.1084/jem.20111457.
41. Bachem A, Guttler S, Hartung E, Ebstein F, Schaefer M, Tannert A, Salama A, Movassaghi K, Opitz C, Mages HW, Henn V, Kloetzel PM, Gurka S, Kroczek RA. 2010. Superior antigen cross-presentation and XCR1 expression define human CD11c+CD141+ cells as homologues of mouse CD8+ dendritic cells. J Exp Med 207:1273–1281. https://doi.org/10.1084/jem.20100348.
42. Supek F, Bosnjak M, Skunca N, Smuc T. 2011. REVIGO summarizes and visualizes long lists of gene ontology terms. PLoS One 6:e21800. https://doi.org/10.1371/journal.pone.0021800.
43. Subramanian A, Tamayo P, Mootha VK, Mukherjee S, Ebert BL, Gillette MA, Paulovich A, Pomeroy SL, Golub TR, Lander ES, Mesirov JP. 2005. Gene set enrichment analysis: a knowledge-based approach for interpreting genome-wide expression profiles. Proc Natl Acad Sci U S A 102:15545–15550. https://doi.org/10.1073/pnas.0506580102.
44. Pantaleo G, Esteban M, Jacobs B, Tartaglia J. 2010. Poxvirus vector-based HIV vaccines. Curr Opin HIV AIDS 5:391–396. https://doi.org/10.1097/COH.0b013e32833d1e87.
45. Sánchez-Sampedro L, Perdiguero B, Mejías-Pérez E, García-Arriaza J, Di Pilato M, Esteban M. 2015. The evolution of poxvirus vaccines. Viruses 7:1726–1803. https://doi.org/10.3390/v7041726.
46. Gomez CE, Najera JL, Krupa M, Perdiguero B, Esteban M. 2011. MVA and NYVAC as vaccines against emergent infectious diseases and cancer. Curr Gene Ther 11:189–217. https://doi.org/10.2174/156652311795684731.
47. Pasparakis M, Vandenabeele P. 2015. Necroptosis and its role in inflammation. Nature 517:311–320. https://doi.org/10.1038/nature14191.
48. Silke J, Rickard JA, Gerlic M. 2015. The diverse role of RIP kinases in necroptosis and inflammation. Nat Immunol 16:689–697. https://doi.org/10.1038/ni.3206.
49. Rock KL, Kono H. 2008. The inflammatory response to cell death. Annu Rev Pathol 3:99–126. https://doi.org/10.1146/annurev.pathmechdis.3.121806.151456.
50. Tam HH, Melo MB, Kang M, Pelet JM, Ruda VM, Foley MH, Hu JK, Kumari S, Crampton J, Baldeon AD, Sanders RW, Moore JP, Crotty S, Langer R, Anderson DG, Chakraborty AK, Irvine DJ. 2016. Sustained antigen availability during germinal center initiation enhances antibody responses to vaccination. Proc Natl Acad Sci U S A 113:E6639–E6648. https://doi.org/10.1073/pnas.1606050113.
51. Postigo A, Cross JR, Downward J, Way M. 2006. Interaction of F1L with the BH3 domain of Bak is responsible for inhibiting vaccinia-induced apoptosis. Cell Death Differ 13:1651–1662. https://doi.org/10.1038/sj.cdd.4401853.
52. Wasilenko ST, Banadyga L, Bond D, Barry M. 2005. The vaccinia virus F1L protein interacts with the proapoptotic protein Bak and inhibits Bak activation. J Virol 79:14031–14043. https://doi.org/10.1128/JVI.79.22.14031-14043.2005.
53. Zhai D, Yu E, Jin C, Welsh K, Shiau CW, Chen L, Salvesen GS, Liddington R, Reed JC. 2010. Vaccinia virus protein F1L is a caspase-9 inhibitor. J Biol Chem 285:5569–5580. https://doi.org/10.1074/jbc.M109.078113.
54. Dai P, Wang W, Cao H, Avogadri F, Dai L, Drexler I, Joyce JA, Li XD, Chen Z, Merghoub T, Shuman S, Deng L. 2014. Modified vaccinia virus Ankara triggers type I IFN production in murine conventional dendritic cells via a cGAS/STING-mediated cytosolic DNA-sensing pathway. PLoS Pathog 10:e1003989. https://doi.org/10.1371/journal.ppat.1003989.
55. Zhang Z, Yuan B, Bao M, Lu N, Kim T, Liu YJ. 2011. The helicase DDX41 senses intracellular DNA mediated by the adaptor STING in dendritic cells. Nat Immunol 12:959–965. https://doi.org/10.1038/ni.2091.
56. Elmore S. 2007. Apoptosis: a review of programmed cell death. Toxicol Pathol 35:495–516. https://doi.org/10.1080/01926230701320337.

57. Swanson CL, Wilson TJ, Strauch P, Colonna M, Pelanda R, Torres RM. 2010. Type I IFN enhances follicular B cell contribution to the T cell-independent antibody response. J Exp Med 207:1485–1500. https://doi.org/10.1084/jem.20092695.
58. Coro ES, Chang WL, Baumgarth N. 2006. Type I IFN receptor signals directly stimulate local B cells early following influenza virus infection. J Immunol 176:4343–4351. https://doi.org/10.4049/jimmunol.176.7.4343.
59. Le Bon A, Schiavoni G, D'Agostino G, Gresser I, Belardelli F, Tough DF. 2001. Type I interferons potently enhance humoral immunity and can promote isotype switching by stimulating dendritic cells in vivo. Immunity 14:461–470. https://doi.org/10.1016/S1074-7613(01)00126-1.
60. Jego G, Palucka AK, Blanck JP, Chalouni C, Pascual V, Banchereau J. 2003. Plasmacytoid dendritic cells induce plasma cell differentiation through type I interferon and interleukin 6. Immunity 19:225–234. https://doi.org/10.1016/S1074-7613(03)00208-5.
61. McLellan JS, Pancera M, Carrico C, Gorman J, Julien J-P, Khayat R, Louder R, Pejchal R, Sastry M, Dai K, O'Dell S, Patel N, Shahzad-Ul-Hussan S, Yang Y, Zhang B, Zhou T, Zhu J, Boyington JC, Chuang G-Y, Diwanji D, Georgiev I, Do Kwon Y, Lee D, Louder MK, Moquin S, Schmidt SD, Yang Z-Y, Bonsignori M, Crump JA, Kapiga SH, Sam NE, Haynes BF, Burton DR, Koff WC, Walker LM, Phogat S, Wyatt R, Orwenyo J, Wang L-X, Arthos J, Bewley CA, Mascola JR, Nabel GJ, Schief WR, Ward AB, Wilson IA, Kwong PD. 2011. Structure of HIV-1 gp120 V1/V2 domain with broadly neutralizing antibody PG9. Nature 480:336–343. https://doi.org/10.1038/nature10696.
62. Bosinger SE, Li Q, Gordon SN, Klatt NR, Duan L, Xu L, Francella N, Sidahmed A, Smith AJ, Cramer EM, Zeng M, Masopust D, Carlis JV, Ran L, Vanderford TH, Paiardini M, Isett RB, Baldwin DA, Else JG, Staprans SI, Silvestri G, Haase AT, Kelvin DJ. 2009. Global genomic analysis reveals rapid control of a robust innate response in SIV-infected sooty mangabeys. J Clin Invest 119:3556–3572. https://doi.org/10.1172/JCI40115.
63. Shannon P, Markiel A, Ozier O, Baliga NS, Wang JT, Ramage D, Amin N, Schwikowski B, Ideker T. 2003. Cytoscape: a software environment for integrated models of biomolecular interaction networks. Genome Res 13:2498–2504. https://doi.org/10.1101/gr.1239303.